Inorganic Chemistry

Article

pubs.acs.org/IC

Linear Dependence of Photoluminescence in Mixed Ln-MOFs for Color Tunability and Barcode Application

Qing-Yuan Yang,[†] Mei Pan,[†] Shi-Chao Wei,[†] Kang Li,[†] Bin-Bin Du,[†] and Cheng-Yong Su*[,‡]

[†]MOE Laboratory of Bioinorganic and Synthetic Chemistry, State Key Laboratory of Optoelectronic Materials and Technologies, Lehn Institute of Functional Materials, School of Chemistry and Chemical Engineering, Sun Yat-Sen University, Guangzhou 510275, China

[‡]State Key Laboratory of Applied Organic Chemistry, Lanzhou University, Lanzhou 730000, China

Supporting Information

ABSTRACT: Multicolored photoluminescence tuning in a single-phase material has invaluable potential in display and security applications. By deliberate design of a multifunctional antenna ligand and precise control of mixed metal ionic compositions in lanthanide metal−organic frameworks (Ln-MOFs), we achieved dichromatic fine-tuning among red, green, or blue primary colors through growth of a series of isomorphous Ln-MOF crystals·solvents of formula $[Ln_nLn'_{1-n}(TTP)_2{\cdot}H_2O]Cl_3$ (Ln = Ln′ = Eu, Tb, and Gd, **1**−**3**; Ln = Eu, Ln′ = Tb, **4**−**8**; Ln = Gd, Ln′ = Eu, **9**−**11**; Ln = Gd, Ln′ = Tb, **12**−**14**; $0 < n < 1$; **TTP** = 1′,1″-(2,4,6-trimethylbenzene-1,3,5-triyl)tris(methylene)tris(pyridine-4(1*H*)-one)). The linear dependence of the emissions were analyzed, and the mathematical matrix models were established, which are useful to control the synthetic conditions and to predict the color chromaticity coordinates under varied excitation wavelengths. The potential relevance of these multicolored photoluminescent Ln-MOFs to barcoded materials was demonstrated.

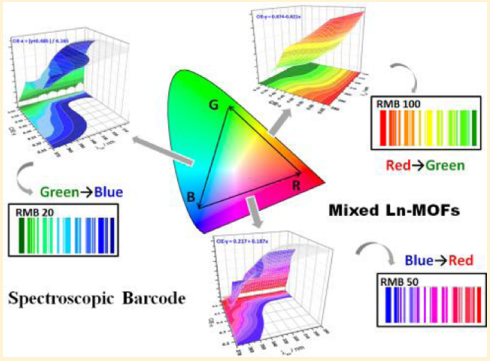

INTRODUCTION

There has been a steady growth of interest in optical materials that can exhibit fine and controllable tunability in photoluminescence, which is useful in a variety of applications, for examlpe, display, lighting, imaging,[1] as well as barcoded materials of security significance.[2] In contrast to traditional semiconductor and inorganic materials to get multicolor-tunable photoluminescence by combining discrete red, green, and blue (RGB) emissive components into a single display unit,[3] in recent years, a promising approach to producing multicolored phosphor in a single-phase material has drawn great attention mainly for the sake of simplicity in fabrication process.[4] Lanthanide (Ln) atoms have natural advantages to meet this purpose owing to their versatile emissions (e.g., red-Eu, green-Tb, and blue-Ce) and narrow band characters.[5] Therefore, a large amount of mixed lanthanide metal−organic frameworks (Ln-MOFs) have been fabricated to tune the photoluminescence through dichromatic or trichromatic strategies,[5,6] which feature in selective incorporation of different Ln centers and chromophoric sensitizers in regular and rigid crystal space to allow dense packing and enhanced emission, meanwhile minimizing self-quenching.[7]

In many cases, luminescence tuning of Ln-MOFs relies on proportional variation of two emissive Ln centers, typically Eu and Tb, in the host frameworks to accomplish dichromatic tunability.[5−8] In a few cases, trichromatic tuning of photoluminescence was obtained by codoping red-Eu and green-Tb into a host framework that can provide dual functions both as photosensitizer and blue chromophore.[9] Nevertheless, in these multicolored photoluminescent systems, precise control of antenna energy transfer (ET) for proportional output of individual colors or linear correlation of color tunability with regard to compositions of individual emissive centers has rarely been examined and established. Such linear dependence for controllable light output is essential to many applications. For example, Rosi and Petoud[2] created a new conceptual luminescent barcoded system with near-IR Ln-MOFs in which the emission bands are linearly correlated to the mixed Ln-atoms ratio. Qian and Chen[10] established excellent linear correlation between temperature and luminescence intensity ratio to create Ln-MOF thermometers.

The common problems of mixed Ln-MOFs that have difficulty in establishing linear correlation for multicolor tunability may include: (1) The ET from f-levels of Tb to those of Eu frequently occurs,[11] which interferes with direct correlation between luminescence intensities and mixed-Ln ratios. (2) Using residual emission of antenna ligand as blue color source is usually concomitant with less ET from the ligand to Ln emitters, thus losing overall emissive efficiency. (3) Doping one Ln atom into the host framework of another Ln atom cannot give a uniform single-phase with the mixed Ln atoms statistically distributed in continuously varied compositions. Therefore, to generate tunable and reproducible

Received: February 4, 2015
Published: March 30, 2015

DOI: 10.1021/acs.inorgchem.5b00271
Inorg. Chem. 2015, 54, 5707−5716

multicolor photoluminescence in linear dependence with mixed Ln-MOFs, the following prerequisites may be required: (1) A versatile antenna ligand competent to simultaneously sensitize Eu and Tb atoms, meanwhile self-emitting blue luminescence independently. (2) Effective multiple ETs to multicomponent emitters irrespective of Ln-mixing and free of self-quenching. (3) Formation of isomorphous heterometallic Ln-MOFs with controllable and adjustable compositions of mixed Ln atoms.[2] We herein report a successful example of linearly multicolor-tunable photoluminescence based on synthesis of a series of heterometallic Ln-MOFs with well-controlled isomorphous compositions. By design of a multifunctional antenna ligand (Figure 1), we succeeded in precise control of dichromatic color-tuning, establishing matrix models for wide range color tunability useful for synthetic prediction and barcoded materials.

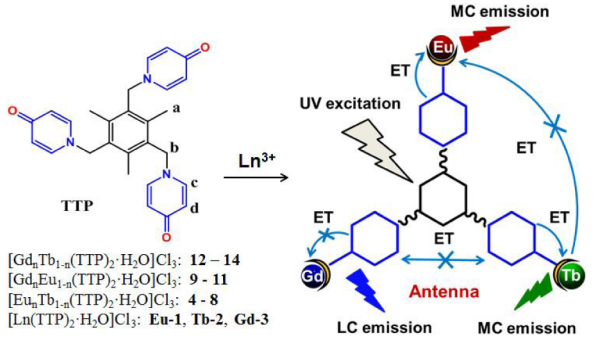

Figure 1. Syntheses of isomorphous Ln-MOFs from a multifunctional TTP ligand that shows multiple antenna effect to independently sensitize emissive red-Eu and green-Tb, while remaining inactive to nonemissive Gd to generate blue self-emission without internal interference between different emissive centers. Eu, Tb, and Gd atoms are used for demonstration of multiple energy-transfer pathways, not the trimetallic complex.

RESULTS AND DISCUSSION

Ligand Design for Multiple Energy Transfer. A bulky semiflexible tripodal ligand 1′,1″-(2,4,6-trimethylbenzene-1,3,5-triyl)tris(methylene)tris(pyridine-4(1*H*)-one) (TTP)[12] bearing a central benzene ring and three pyridone donors was designed as organic antenna (Figure 1). This molecule is neutral and able to present tautomeric transformation between the charge-separated and the keto forms (Supporting Information, Figure S2), possessing two types of aromatic motifs connected through unconjugated methylene $-CH_2-$ linkages. We analyzed the single-crystal structure of the pure ligand (Supporting Information, Figure S3), confirming that free ligand TTP is dominantly in keto form, which is also in agreement with the density functional theory (DFT) calculations (Supporting Information, Figure S6). It is known that the pyridone units in this kind of ligand are blue-emissive in the keto form, while the charge-separated form is nonemissive. The DFT calculations disclose that the highest occupied molecular orbitals (HOMOs) are mainly contributed by the π orbitals on terminal O or pyridone rings, while the lowest unoccupied molecular orbitals (LUMOs) include π^* orbitals of the central benzene ring (Supporting Information, Figure S7). This suggests that the intraligand charge transfer (ILCT) involving pyridone rings, central benzene ring, and heteroatom O may take place, besides separate $\pi \rightarrow \pi^*$ transitions localized within three individual pyridone rings and the central benzene ring.[13]

Owing to the above unique molecular nature, the ligand TTP may be able to provide multiple independent ET (ET) pathways suitable for sensitizing multicomponent emissive centers (e.g., coordination to both Eu and Tb), as well as self-emission if anyone of ET pathways is blocked (e.g., coordination to Gd). Such organic photosensitizer integrating separate antenna effects and blue self-emission is specifically suitable for linearly dependent multicolor photoluminescence of mixed Ln-MOFs, because each individual ET and emission is independent to avoid interference from others. As demonstrated by an idealized sensitizing model in Figure 1, TTP may sensitize different Ln atoms simultaneously but independently, for example, Eu and Tb, once they are coordinated to different pyridone donors. The individual ET from every terminal donor to its bonding Ln atom also prevents intramolecular quenching because they are far separated by unconjugated methylene $-CH_2-$ groups linking to the central benzene, thus effectively retarding the Dexter ET between different metal sites. On the other hand, if anyone of pyridone donors is bonded to a nonradiative Gd atom, blue ligand emission can be regenerated without disturbing the other two donors to sensitize bonding Eu or Tb atoms. Therefore, such multiple ET pathways in TTP ligand could effectively activate multicomponent emissions by avoiding above-mentioned problems in common conjugated monofunctional antenna system that often causes energy loss and self-quenching.

Crystal Growth of Isomorphous Ln-MOFs. A key step to generate linearly dependent multicolor photoluminescence by the mixed-Ln-MOFs is to incorporate different Ln atoms into the same coordination framework in the desired proportions with the uniform structure integrity and statistic space distribution. Since Eu^{3+}, Gd^{3+}, and Tb^{3+} ions have resembling ionic radii (1.066, 1.053, and 1.040 Å with CN = 8), and ligand TTP is semiflexible to be able to tolerate slight coordination bond variation, formation of both monometallic and heterometallic Ln-MOFs in isomorphous structures is expectable.[14] Indeed, reactions of TTP with $LnCl_3·6H_2O$ in uniform and mixing conditions readily afforded various mono- and bimetallic isostructural Ln-MOFs as listed in Figure 1 and Table 1, showing general formula $[\mathbf{Ln_nLn'_{1-n}(TTP)_2·H_2O}]\mathbf{Cl_3}$·solvents (Ln = Ln′ = Eu, Tb, or Gd, **1**−**3**; Ln = Eu, Ln′ = Tb, **4**−**8**; Ln =

Table 1. Synthesis and Lifetime Information

			τ (ms)	
complexes	feeding ratios	metal ratios from EDX	Eu^{3+}	Tb^{3+}
1	100	**Eu**	0.41(1)	
2	100	**Tb**		0.73(2)
3	100	**Gd**		
4	0.65:0.35	$\mathbf{Eu_{0.66}Tb_{0.34}}$	0.40 (2)	0.69 (3)
5	0.55:0.45	$\mathbf{Eu_{0.53}Tb_{0.47}}$	0.41 (2)	0.73 (3)
6	0.45:0.55	$\mathbf{Eu_{0.44}Tb_{0.56}}$	0.41 (2)	0.77 (3)
7	0.30:0.70	$\mathbf{Eu_{0.30}Tb_{0.70}}$	0.44 (2)	0.78 (3)
8	0.15:0.85	$\mathbf{Eu_{0.17}Tb_{0.83}}$	0.48 (2)	0.78 (3)
9	0.70:0.30	$\mathbf{Gd_{0.76}Eu_{0.24}}$	0.41 (1)	
10	0.50:0.50	$\mathbf{Gd_{0.51}Eu_{0.49}}$	0.40 (1)	
11	0.35:0.65	$\mathbf{Gd_{0.33}Eu_{0.67}}$	0.40 (1)	
12	0.65:0.35	$\mathbf{Gd_{0.67}Tb_{0.33}}$		0.72 (2)
13	0.55:0.45	$\mathbf{Gd_{0.57}Tb_{0.43}}$		0.72 (2)
14	0.45:0.55	$\mathbf{Gd_{0.41}Tb_{0.59}}$		0.72 (2)

DOI: 10.1021/acs.inorgchem.5b00271
Inorg. Chem. 2015, 54, 5707−5716

Gd, Ln′ = Eu, **9**−**11**; Ln = Gd, Ln′ = Tb, **12**−**14**; $0 < n < 1$). All complexes were obtained as crystal products, and their molecular structures and phase purities were identified by representative powder and single-crystal X-ray diffraction (XRD) measurements (Figures 2 and 3 and Supporting Information, Figures S8−S11), respectively. For bimetallic complexes, the mixed Ln atomic compositions were checked by energy-dispersive X-ray spectroscopy (EDX) with two independently synthesized crystalline samples for each complex (Supporting Information, Table S1). The results verify reproducible syntheses of mixed-Ln-MOFs, indicating formation of isomorphous structures with any desired Ln mixing concentrations in a predictable fashion simply by controlling the stoichiometry of feeding metals. Thermal gravimetric analysis (TGA) denotes that the crystalline products are stable up to 330 °C, and all lattice solvents could be evacuated upon heating to ∼100 °C (Supporting Information, Figure S12). The detailed synthesis and characterization information are listed in Supporting Information.

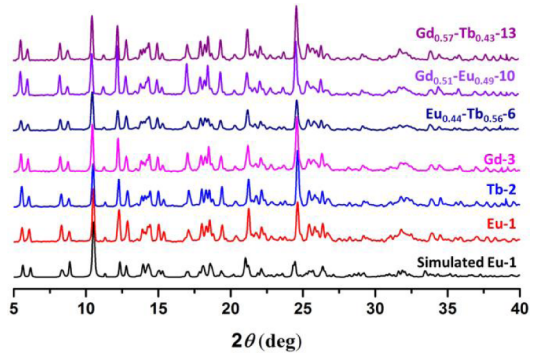

Figure 2. Powder XRD patterns of the monometallic complexes **1**−**3** and the representative bimetallic complexes **6**, **10** and **13** in comparison with the single-crystal data simulation.

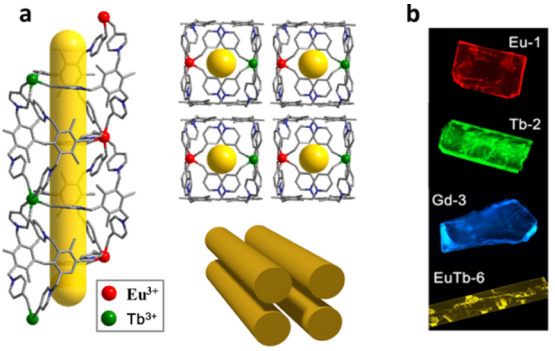

Figure 3. (a) Crystal structure of isomorphous complexes showing 1D tubular chain and packing mode. Distribution of Ln^{3+} ions demonstrated in different colors. (b) Real images of single-crystals emitting different colors (λ_{ex} = 340−380 nm).

The spatially regular disposition of Ln atoms and antenna ligands was unambiguously established by the single-crystal X-ray analyses of the monometallic complexes **1**−**3** and bimetallic complexes **6**, **10**, and **13** (Supporting Information, Tables S2 and S3), together with screening of unit cell parameters for all complexes. Isostructural nature of both mono- and bimetallic complexes are well established, all crystallizing in the same chiral space group $P2_1$. In general, the asymmetric unit consists of crystallographically independent one Ln^{3+}, two TTP, three noncoordinating Cl^-, one coordinating H_2O, and some solvent molecules. As depicted in Figure 3, each Ln^{3+} ion shows a pentagonal−bipyramidal geometry coordinated by seven O atoms from six different TTP ligands and one water molecule, while each TTP ligand connects three different Ln^{3+} ions. One-dimensional (1D) chain is thus generated, which can be envisaged as a right-handed triple-stranded helix running along the crystallographically imposed 2_1 axis with a pitch of 41.5 Å. Surrounding of TTP ligands and Ln ions around the 2_1 axis forms a hollow cylinder tube, leaving spacious voids with Ln−Ln separation of 11.5−13.8 Å. Such 1D tubes are further arranged in parallel in the crystal lattice to give a periodically ordered architecture, consolidated by formation of intermolecular $\pi\cdots\pi$ interactions and hydrogen bonds among water solvents and Cl^- anions. For the mixed-Ln-MOFs, the corresponding Ln^{3+} content in each crystal was designated on the basis of EDX analytic results (vide infra). It is noticeable that the C−O bond lengths in all complexes fall in the range of 1.208−1.296 Å, which are typical of C═O double bond (∼1.20 Å) rather than C−O single bond (∼1.43 Å), indicating that the TTP ligands are dominated in keto form in all cases.

Owing to the perfect crystallinity and X-ray scattering, detailed analysis of the single-crystal data of the bimetallic complexes (**6**, **10**, and **13**) in comparison to those of monometallic complexes (**1**−**3**) can afford specifically valuable solid-state structural information. Figure 4 illustrates plots of the unit cell parameters, crystallographically identical Ln−O bonds, and ideal Ln^{3+} ionic radii of all measured single-crystals versus Ln^{3+} ions variation in different complexes. The constant *a*, *b*, and *c* cell parameters irrespective of Ln^{3+} ion variation verify that the present Ln-MOF structural model has excellent three-dimensional (3D) space tolerance against replacing or mixing of different Ln^{3+} ions (Figure 4b), making it possible to quantitatively form isomorphous mixed-Ln-MOF crystals in any desired Ln atoms composition. Moreover, the corresponding Ln−O bond distances (Figure 4c) in both monometallic and bimetallic complexes are exactly correlated with the idealized Ln^{3+} ionic radii (Figure 4d) in terms of plotted trend lines versus Ln^{3+} ions variation. Such exact matching of the crystallographic data evidently supports success of the present crystal growth method for construction of isomorphous mixed-Ln-MOFs, in which different Ln^{3+} ions are perfectly distributed in the crystal lattice, consistent with the EDX analytic results. The uniform distribution of the mixed Ln^{3+} ions in a bimetallic crystal can also be directly seen from the luminescent image of the single-crystal $\mathbf{Eu_{0.44}Tb_{0.56}}$-**6** (Figure 3b), of which the whole crystal emits pure yellow color obviously contributed by the uniformly mixed Eu^{3+} and Tb^{3+} ions in the crystal lattice. These structural features manifest a repeatable crystal engineering process to grow heterometallic crystals with continuous isomorphous replacement of Ln^{3+} ions, which is crucial for multicolored photoluminescence and tunability by means of assembling mixed-Ln-MOFs in a single phase.

Color Tunability and Correlation Matrix. As shown in Figure 5 and Supporting Information, Figure S13, the free ligand TTP shows blue luminescence with one unsymmetric wide band around 445 nm. The biexponential lifetimes (τ = 1.8 and 6.3 ns) unveil manifold emission pathways of TTP, probably dominated by ligand-centered (LC) $\pi^* \rightarrow \pi$ transitions in the keto form of pyridone donors and other intraligand charge-transfer (ILCT) processes,[13] in accord with above DFT calculations. In monometallic complexes **Eu-1** and

DOI: 10.1021/acs.inorgchem.5b00271
Inorg. Chem. 2015, 54, 5707−5716

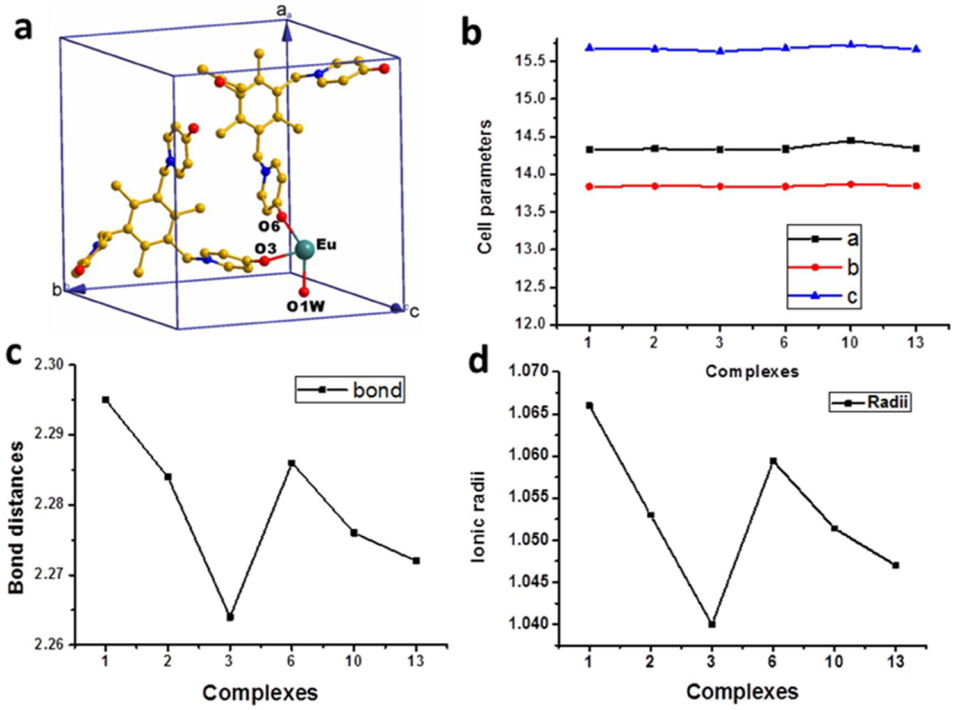

Figure 4. Structural parameters comparison for complexes **1**−**3**, **6**, **10**, and **13**. (a) Unsymmetric molecular structure in a unit cell. (b) Cell parameters. (c) Crystallographicall identical Ln−O bond distances. (d) Ideal Ln^{3+} ionic radii in mono- and bimetallic Ln-MOFs (normalized for mixed Ln^{3+} ions according to corresponding Ln^{3+} content in mixed-Ln-MOFs **6**, **10**, and **13**).

Tb-2, these ligand-based emissions are suppressed. Instead, series of sharp peaks characteristic of red-Eu and green-Tb metal-centered (MC) luminescence appear, corresponding to $^5D_0 \rightarrow {}^7F_J$ (J = 1−3) transitions for Eu^{3+} and $^5D_4 \rightarrow {}^7F_J$ (J = 6−3) transitions for Tb^{3+}, respectively. The lifetime of Eu^{3+} is 0.41(1) ms at 613 nm, and that of Tb^{3+} is 0.73(2) ms at 542 nm (Table 1 and Supporting Information, Table S4), typical of normal f-level excited states. In both cases, suppression of ligand emission is suggestive of effective ET from ligand adsorption to f-levels of Eu^{3+} and Tb^{3+}, confirming competent antenna effect of TTP. On the other hand, complex **Gd-3** shows blue luminescence with a broad band centered at 457 nm, comparable with the ligand-based emissions and verified by the short lifetimes (τ = 1.3 and 2.7 ns) similar to that of free ligand TTP. This means that ET from the ligand excited state to Gd^{3+} f-levels (>31 000 cm^{-1}) cannot take place, thus regenerating blue LC emission of the ligand. The triplet T_1 states of TTP were estimated by phosphorescence spectra of **Gd-3** at 77 K (Figure S14), revealing a broad band with onset at 26 700 and major peak at 20 300 cm^{-1} (τ = 0.35 ms). This may account for efficient sensitization of both Eu^{3+} and Tb^{3+} emissions with reasonable energy difference ΔE ($Eu^{3+}{}^5D_0$ = 17 400 and $Tb^{3+}{}^5D_4$ = 20 400 cm^{-1}). For example, the overall sensitization efficiency (η_{sens}) of Eu^{3+} centers in complex **Eu-1** can be estimated at 43% based on the spectral data and the measured overall quantum yield (Q_L^{Eu} = 11%), and this is even higher for complex **Tb-2** (>70% according to Q_L^{Tb} = 70%).[1d,15] A potential sensitization mechanism showing various ET processes is illustrated in Figure 5f.

On the basis of three primary RGB colors emitted by **Eu-1**, **Tb-2**, and **Gd-3**, it is expected to produce multicolored photoluminescence by integrating different Ln^{3+} ions into a single-crystal of mixed-Ln-MOF. The dichromatic approach has been tested to fine-tune RG, GB and BR luminescence by synthesis of three series of bimetallic complexes. As shown in Figure 5 and Supporting Information, Figures S15−16, the $\mathbf{Eu}_n\mathbf{Tb}_{1-n}$ series crystals (**4**−**8**) display sharp characteristic emission peaks from both Eu^{3+} and Tb^{3+} centers. The excitation spectra monitored at respective Eu^{3+} and Tb^{3+} emission peaks display two overlapped bands with maxima centering at 290 and 283 nm (Supporting Information, Figure S15). This evidently indicates that the ligand TTP embedded in Eu/Tb-mixed Ln-MOFs is able to sensitize these two Ln^{3+} centers simultaneously. Excitations through these bands can directly produce dual MC emissions of red-Eu and green-Tb. As expected, by increasing the amount of Eu^{3+} while proportionally decreasing the amount of Tb^{3+} in mixed-Eu/Tb-MOF crystals, the red-emission intensity was increased, while that of green-emission decreased accordingly. This enables color tuning in the RG spectral region simply by changing the metal ratios in the single crystal. As depicted in Figure 5b,e and Supporting Information, Figure S16, the emission colors and the chromaticity coordinates in the 1931 CIE diagram can be systematically tuned with precise correlation to the Eu/Tb ratios. Furthermore, since the excitation spectra of Eu^{3+} and Tb^{3+} are overlapped but not completely superimposed, varying the excitation wavelengths along this region will also produce color change owing to different ET efficiency to Eu^{3+} or Tb^{3+} ions (Supporting Information, Figure S16b). It is noteworthy that no significant lifetimes increase of Eu^{3+} or decrease of Tb^{3+} are observed in these mixed-Eu/Tb-MOF crystals in comparison to the pure **Eu-1** and **Tb-2** (Table 1). This strongly indicates that the commonly encountered crossing ET from Tb^{3+} to Eu^{3+} does not occur here,[10,11] which allows for excellent linear correlation in color tunability that is of crucial importance to color control and application in barcoded materials discussed below.

DOI: 10.1021/acs.inorgchem.5b00271
Inorg. Chem. 2015, 54, 5707−5716

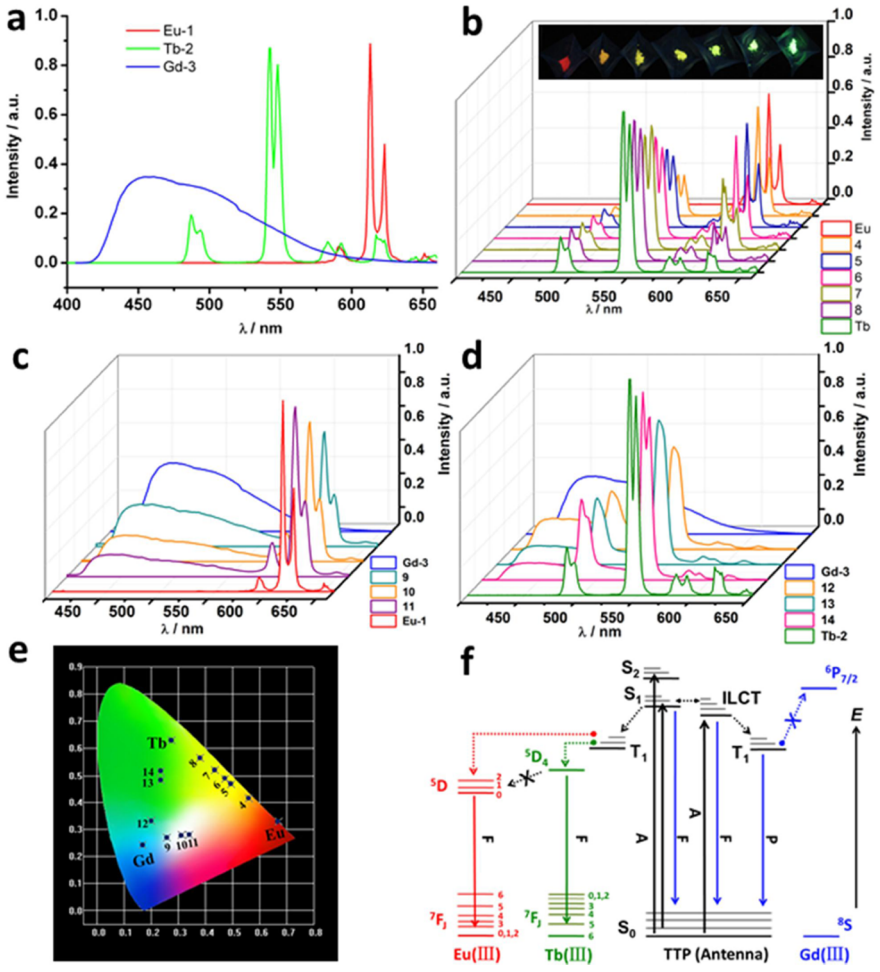

Figure 5. Solid-state emission spectra of monometallic complexes **1**−**3** (a), bimetallic $\mathbf{Eu}_n\mathbf{Tb}_{1-n}$ **4**−**8** in comparison to **1** and **2** (λ_{ex} = 290 nm) with inset showing emissive photographs of bulk samples (b), bimetllic $\mathbf{Eu}_n\mathbf{Gd}_{1-n}$ **9**−**11** in comparison to **1** and **3** (λ_{ex} = 365 nm) (c), and bimetallic $\mathbf{Tb}_n\mathbf{Gd}_{1-n}$ **12**−**14** in comparison to **2** and **3** (λ_{ex} = 365 nm) (d). (e) The CIE coordinates for all complexes. (f) Schematic representation of photophysical processes. A, absorption; F, fluorescence; P, phosphorescence; S, singlet; T, triplet; ILCT, intraligand charge transfer; E, energy. Back transfer processes are not drawn for the sake of clarity.

The color-tuning in the BR and GB spectra regions was also tested by preparation of $\mathbf{Gd}_n\mathbf{Eu}_{1-n}$ series (**9**−**11**) and $\mathbf{Gd}_n\mathbf{Tb}_{1-n}$ series (**12**−**14**) isomorphous crystals, respectively (Figure 5c,d and Supporting Information, Figures S17 and S18). In contrast to those of $\mathbf{Eu}_n\mathbf{Tb}_{1-n}$ bimetallic complexes in which the overall color is determined by the narrow MC emissions, the optic spectra of these two series display both MC and LC luminescence. $\mathbf{Gd}_n\mathbf{Eu}_{1-n}$ crystals emit the characteristic photoluminescence of Eu^{3+} similar to that of **Eu-1**, and the ligand-based emission with a broad band centered at 457 nm resembling that of **Gd-3**. Similarly, the emission spectra of $\mathbf{Gd}_n\mathbf{Tb}_{1-n}$ crystals also show the characteristic $^5D_4 \rightarrow {}^7F_J$ transitions of Tb^{3+} similar to those of **Tb-2**, and the broad emission related to $\mathbf{Gd}^{3+}$ coordination component. As expected, by altering the Eu/Gd or Tb/Gd metal ratios, the MC luminescence intensities increase or decrease accompanied by consequent decreasing or increasing of LC emissions. Therefore, emission colors of these bimetallic complexes can be tuned from red to blue or green to blue simply by changing the mixed Ln^{3+} compositions (Figure 5e). In all cases, the lifetimes of Eu^{3+} and Tb^{3+} emission components in bimetallic complexes are closely comparable with those of monometallic complexes (Table 1), strongly suggesting that the multiple ET pathways in TTP are independent without intramolecular self-quenching or crossing migration (e.g., Tb^{3+} to Eu^{3+} transfer).[10,11]

From the above discussion we can see that color tuning between every two RGB primary colors is achievable through preparation of bimetallic complexes incorporating any two of three Ln ions of Eu^{3+}, Tb^{3+}, and Gd^{3+}. Two types of color tuning techniques may be applied: (1) varying the relative contents of Ln ions in the mixed Ln-MOFs crystals and (2) adjusting the exciting wavelengths along the overlapped excitation spectral range. Figure 6a collects the Commission International de l'Eclairage (CIE) chromaticity coordinates of all mono- and bimetallic complexes, constituting a triangle spanning a wide region to cover three primary RGB colors. To check if the triangle diagram is applicable to the practical fine-tuning of emission colors via the dichromatic approach, we also measured photoluminescence of three bimetallic series by systematically varying the excitation wavelengths. The resulting data from all complexes and excitations are listed in Supporting Information, Tables S5−S7, which were thoroughly analyzed and illustrated in Figure 6 and Supporting Information, Figures S20−S31.

As seen from Figure 6 and Supporting Information, Figures S20−23, analysis of the chromaticity coordinates (*x*,*y*) from various emissions of $\mathbf{Eu}_n\mathbf{Tb}_{1-n}$ complexes, including those of

DOI: 10.1021/acs.inorgchem.5b00271
Inorg. Chem. 2015, 54, 5707−5716

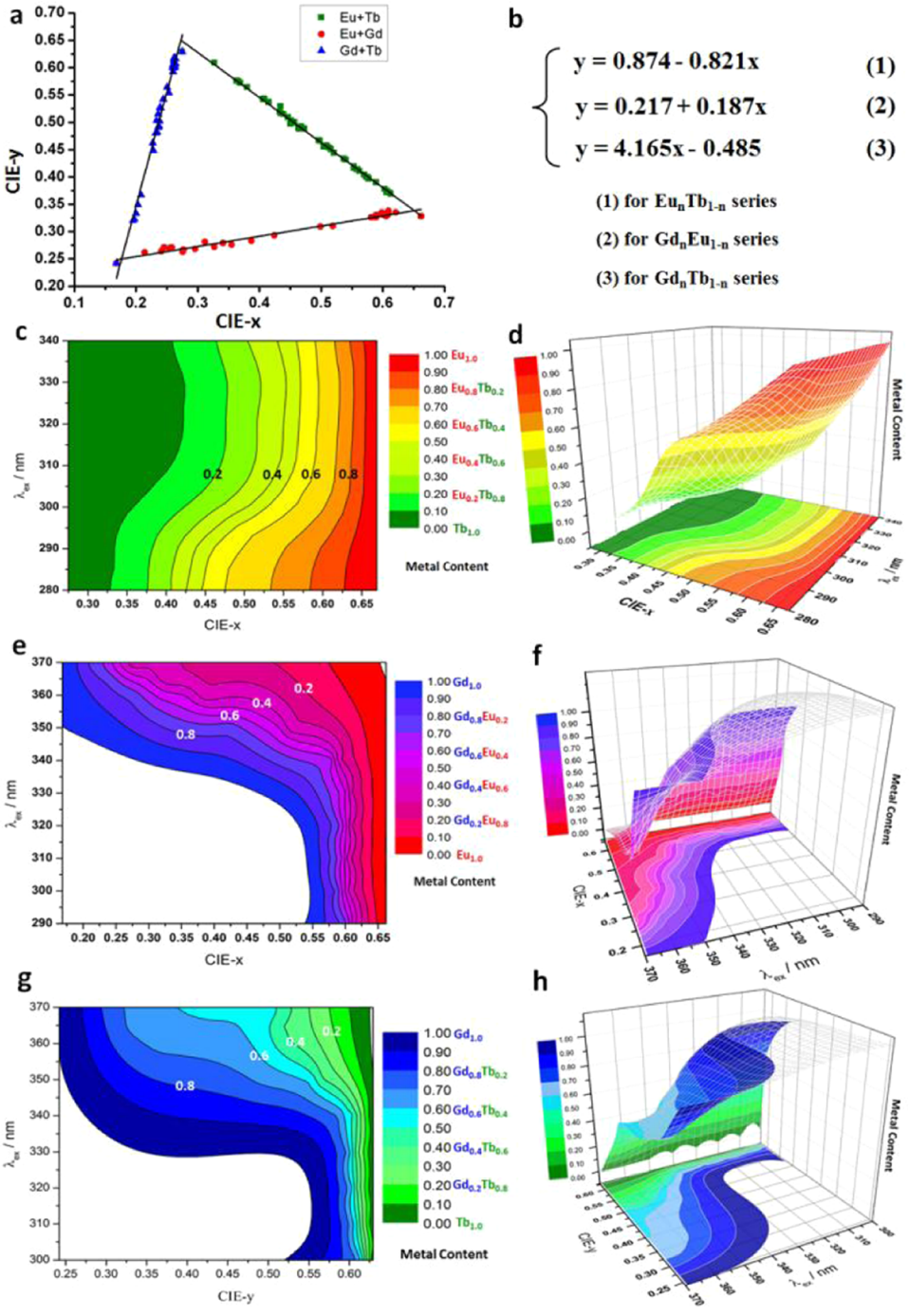

Figure 6. (a) The linear fitting graph of CIE coordinates of three series bimetallic complexes (**4**−**14**) excited at various wavelengths, showing a triangle with three meeting points approaching to RGB colors of monometallic complexes **1**−**3**. (b) Linear correlations of CIE coordinates with metal compositions in three series of bimetallic complexes. (c−h) 2D and 3D matrix models correlating CIE coordinates, excitation wavelengths, and metal contents. The *x*-axis represents the CIE-*x* or CIF-*y* values. (The corresponding CIE-*y* or CIE-*x* values can be calculated from eqs 1−3, respectively.) The *y*-axis represents the different excitation wavelengths. The *z*-axis or color bar represents the percentages of mixing Ln^{3+} ions. The color bars, corresponding to color gradients in 2D and 3D matrices, refer to metal compositions, not real emission colors.

Eu-1 and **Tb-2**, establishes a perfect linear relationship expressed by the equation $y = 0.874-0.821x$ (Figure 6b). This allows generation of a two-dimensional (2D) matrix model demonstrating the relationship among the excitation wavelengths, emission colors, and Ln^{3+} compositions in **Eu$_n$Tb$_{1-n}$** series (Figure 6c). From this modeling diagram, the chromaticity coordinate (i.e., emission color) of any defined **Eu$_n$Tb$_{1-n}$** complex at a specific exciting wavelength can be easily read. More accurately, a 3D matrix model may be constructed once enough photoluminescent data are available (Figure 6d), which can facilitate even precise readout of the information with regard to emissions, excitations, and metal ratios. The 2D matrix model can be considered as the simplified projection of the 3D matrix model in the *xy* plane. Similarly, 2D and 3D matrix models for **Gd$_n$Eu$_{1-n}$** and **Gd$_n$Tb$_{1-n}$** series also were constructed according to the linear relationship expressions $y = 0.217 + 0.187x$ and $y = 4.165x - 0.485$, respectively, suggesting that correlation of CIE coordinates for

DOI: 10.1021/acs.inorgchem.5b00271
Inorg. Chem. 2015, 54, 5707−5716

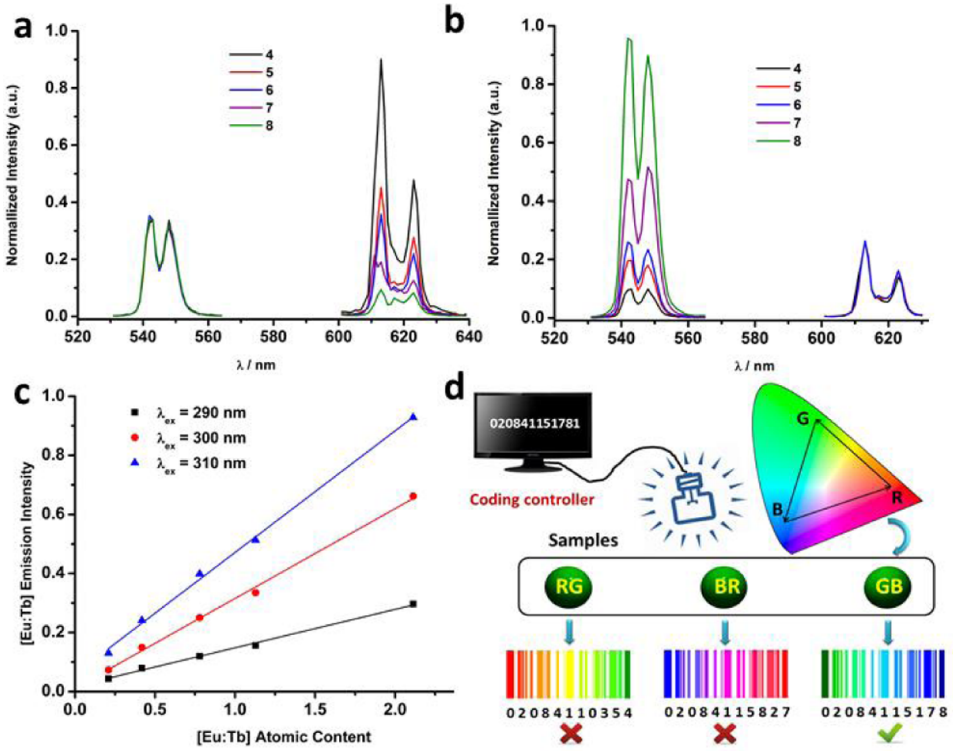

Figure 7. (a) Emission intensities variation of Eu^{3+} (613 nm) normalized to those of Tb^{3+} (542 nm), and (b) emission intensities variation of Tb^{3+} (542 nm) normalized to those of Eu^{3+} (613 nm) for binary $\mathbf{Eu}_n\mathbf{Tb}_{1-n}$ series **4**–**8**. (c) Plots of the ratios of integrated emission intensities vs Eu/Tb metal ratios (black, λ_{ex} = 290 nm; red, λ_{ex} = 300 nm; blue, λ_{ex} = 310 nm). Excitation at each specific wavelength produces concurrent Eu^{3+} and Tb^{3+} emissions that are linearly correlated to the Eu/Tb metal ratios. (d) Demonstration of using the present mixed-Ln-MOFs as linearly adjustable luminescent materials for encryption strips and anticounterfeiting technology with numerous possible encoding combinations.

these two series of bimetallic complexes (Figure 6e–h and Supporting Information, Figures S24–S31) is possible. However, notice that the correlation coefficients in $\mathbf{Gd}_n\mathbf{Eu}_{1-n}$ and $\mathbf{Gd}_n\mathbf{Tb}_{1-n}$ series (Figures S25 and S29) are relatively unsatisfactory in contrast to $\mathbf{Eu}_n\mathbf{Tb}_{1-n}$ series, which implies less certainty of linear dependence of RB and GB color tuning. The main reason is due to the broad nature of the blue LC emissions, which is subject to subtle environment influence and of less quantitative precision compared with the well-protected f–f MC emissions. Further study is underway for better data analyses and improvement.

The matrix models established for these mixed Ln-MOFs not only prove validity of emission fine-tuning among RG, RB, and GB colors through a dichromatic approach but also provides an useful tool to accurately determine the CIE coordinates of mixed-Ln-MOFs from their metal compositions and exciting wavelengths. On the other hand, these matrix models can also be used as a guidance to predict the synthetic conditions of mixed-Ln-MOFs for any desired luminescence as demonstrated in Supporting Information, Figure S32. For example, to achieve a yellow emission at CIE coordinate (0.50, 0.46), we can conveniently choose any of the following methods: (1) prepare the bimetallic complex with metal content of $Eu_{0.64}Tb_{0.36}$ and excite at 285 nm, (2) prepare the bimetallic complex with metal content of $Eu_{0.53}Tb_{0.47}$ and excite at 295 nm, (3) prepare the bimetallic complex with metal content of $Eu_{0.32}Tb_{0.68}$ and excite at 305 nm, or (4) prepare the bimetallic complex with metal content of $Eu_{0.25}Tb_{0.75}$ and excite at 330 nm. In other words, the matrix models can easily tell us how to determine the CIE coordinates of bimetallic complexes containing different metal compositions when excited at a specific wavelength or how to prepare bimetallic complexes that can emit a specific color by mixing different metal ions and exciting at proper wavelengths.

Potential Barcode Application. An ideal barcoded material should possess competent characters such as good stability, easy preparation, high reproducibility, innumerous encoding combinations, straightforward recognition, as well as rapid but unambiguous interpretation of spectral signature by inexpensive equipment.[2] On the basis of the above discussion, we can see that these required qualities could be well-met by the present mixed-Ln-MOFs with the isomorphous structures easily subject to continuous metal ions replacement.

Since the linear dependence of the light output is of significance to the reliable coding and decoding, we chose the bimetallic $\mathbf{Eu}_n\mathbf{Tb}_{1-n}$ series complexes for further analyses to demonstrate how their linearly adjustable luminescence endows them with potential for use as barcoded materials. First, we know that all CIE coordinates (x, y) of $\mathbf{Eu}_n\mathbf{Tb}_{1-n}$ complexes of any varied Eu/Tb ratios should fall in the line between **Eu-1** and **Tb-2** defined by the linear equation $y = 0.874-0.821x$ (Figure 6a,b) and are inherently correlated to specific excitation wavelengths and Ln^{3+} compositions defined in the 2D and 3D matrices (Figure 6c,d). Second, the color components contributing to the emission tunability also show linear dependence on the Eu/Tb variations. As shown in Figure 7, after normalizing the emission intensities of the main peak of Tb^{3+} (542 nm) to those of Eu^{3+} (613 nm), or vice versa, plots of the ratios of the integrated emission intensities with respect to the Eu/Tb ratios display exact linear relationship. However, because of different ET efficiency to Eu^{3+} or Tb^{3+} ions at varied excitations (Supporting Information, Figure S16b), distinctive trendlines can be obtained at different excitations (Figure 7c).

DOI: 10.1021/acs.inorgchem.5b00271
Inorg. Chem. 2015, 54, 5707–5716

This is of special interest because multiple detections are offered to verify the authenticity of an encryption tag made from the same series of Eu_nTb_{1-n} complexes.

On the basis of above analyses, preparation of desired isomorphous Eu_nTb_{1-n} complexes for encoding strategy is easy to proceed. For the sake of simplicity, we define three color bars at yellow (0.45, 0.50), orange (0.54, 0.43), and red (0.61, 0.37). From the 2D matrix shown in Figure 8, we can easily

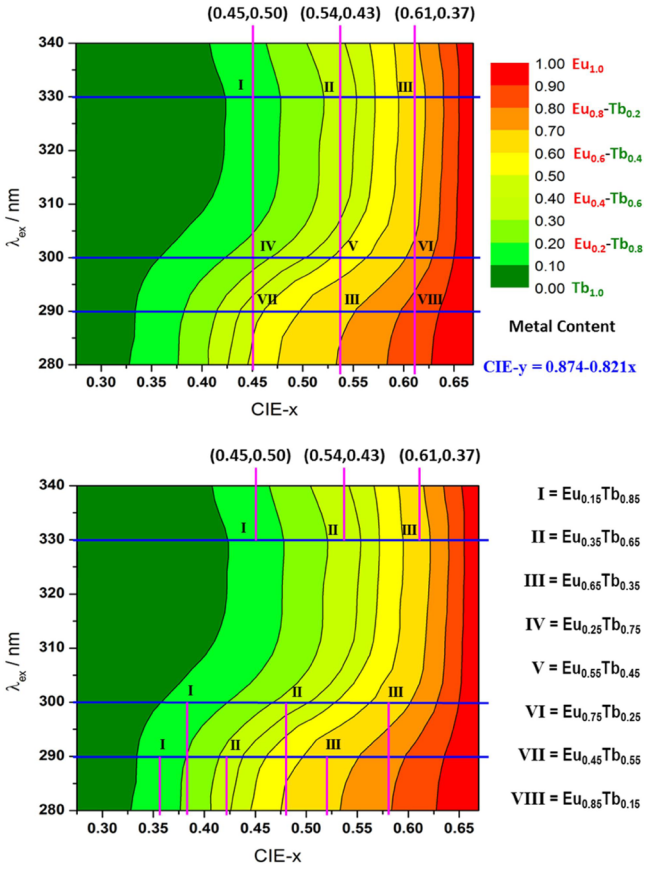

Figure 8. Demonstration on how to use the 2D correlation matrix of Eu_nTb_{1-n} complexes in synthetic control and optic parameters readout. (upper) Blue lines show how to obtain different CIE coordinates at a selected excitation by preparing mixed-Ln-MOF containing desired metal ratios, and purple lines show how to obtain the same CIE coordinate (emission color) from mixed-Ln-MOFs containing different metal ratios by selecting proper exciting wavelength. Each crossing point defines a set of parameters including excitation wavelength, emission color, and metal ratio. (lower) How to read CIE coordinates of three predefined Eu_nTb_{1-n} complexes at different excitations.

determine various feed ratios of Eu/Tb for materials syntheses. For example, we can obtain three series of Eu_nTb_{1-n} complexes, (I, II, III), (IV, V, VI), and (VII, III, VIII), to achieve these three defined colors at excitations of 330, 300, and 290 nm, respectively. This means we are able to design as many as code combinations between Eu/Tb compositions and excitation wavelengths for a set of predefined color bars. On the other hand, for each series of isostructural Eu_nTb_{1-n} complexes, their color bars can be further altered by variation of excitation wavelengths. For example, the same series Eu_nTb_{1-n} complexes I–III could afford three different sets of color bars when excited at three different wavelengths, which can be readily read from the 2D matrix (Figure 8) as listed in Table 2. This means we are able to design as many as code combinations between emission colors and excitation wavelengths for a set of predefined Eu_nTb_{1-n} complexes.

Table 2. Representative Readout Information from the 2D Correlation Matrix of Eu_nTb_{1-n} Series Complexes

	CIE		
λ (nm)	(0.45, 0.50)	(0.54, 0.43)	(0.61, 0.37)
330	I	II	III
300	IV	V	VI
290	VII	III	VIII
		complex	
λ (nm)	I	II	III
330	(0.45, 0.50)	(0.54, 0.43)	(0.61, 0.37)
300	(0.38, 0.56)	(0.48, 0.48)	(0.58, 0.40)
290	(0.36, 0.58)	(0.42, 0.53)	(0.52, 0.45)

Moreover, since the bimetallic Eu_nTb_{1-n} complexes can be facilely synthesized with high repeatability in actually unlimited Eu/Tb mixing ratios, numerous metal compositions for possibly innumerable encoding combinations may be envisaged. Owing to the good linear relationship of CIE coordinates upon excitation and Eu/Tb variations (Figures 6a,b), exact correlation of three encode elements, that is, CIE coordinates, metal compositions, and excitation wavelengths, can be expressed by a matrix model and used directly as encoder matrix (Figures 6c,d and 8). Although we only demonstrate a very simple encoding strategy (Table 2) by a rough 2D correlation matrix (Figure 8), which was generated by limited Eu_nTb_{1-n} complexes, more precise 3D matrix can be expected if sufficient Eu_nTb_{1-n} complexes could be tested under small enough excitation intervals, which may provide an accurate encoding model with large code capacity for barcode computing. On the other hand, since three encode elements are inherently correlated but variable with mutual dependency, it is easy to define one set of element while generating the other two sets of elements arbitrarily. For example, Table 2 lists two representative encoding strategies. We can define three color bars as the fixed set of encode element while generating different combinations of excitation and Eu/Tb variations as the other two sets of variable encode elements. Similarly, if three bimetallic complexes (I–III) are chosen as the fixed encode element, different combination of excitation and CIE coordinates could be generated as the variable encode elements. Since the color tunability was proven to be in linear dependence on the Eu/Tb metal ratios at each excitation wavelength (Figure 7c), generation of different combinations of variable encode elements (e.g., excitations vs CIE coordinates) for a set of predefined encode element (e.g., complexes I–III) can be reliably considered as the multiple detections for authentic verification and validation. This implies a high encryption technique for anticounterfeit technology and true-or-false identification (Supporting Information, Figures S33 and S34).

Finally, the visible photoluminescent colors emitted by the mixed-Ln-MOFs make the spectral signature easily and rapidly acquirable and interpretable by the portable spectrometers, or even by naked eyes, and their inner-shell f–f luminescence also makes Ln-based barcoded materials undisturbed by environmental interference. Therefore, the present mixed-Ln-MOFs might find promising potentials in secure optical devices, encryption tags, and anticounterfeit technologies as demon-

DOI: 10.1021/acs.inorgchem.5b00271
Inorg. Chem. 2015, 54, 5707–5716

strated in Figure 8 and Supporting Information, Figures S33 and S34.

CONCLUSIONS

In summary, by designing a multifunctional ligand suitable for photosensitization of multicomponent phosphor as well as blue self-emission, we succeeded in crystal engineering of isomorphous mixed-Ln-MOFs that can emit multicolored photoluminescence and achieve linear color tunability. On the basis of the isostructural monometallic complexes of Eu^{3+}, Tb^{3+}, and Gd^{3+}, which are qualified as RGB primary emitters, combination of any two of these three Ln^{3+} ions in bimetallic complexes allows for dichromatic fine-tuning of RG, GB, and BR colors. We have demonstrated that, by simple control of reactant stoichiometry, it is possible to reproducibly alter the Ln^{3+} ion compositions in bimetallic complexes and therefore control the resulting individual emission intensities in a linear fashion. In this way, we can fine-tune the emission colors along the RGB triangle simply by altering the relative metal content and changing the excitation wavelengths. The good linear correlation of the chromaticity coordinates in all complexes makes it possible to set up matrix models to correlate the excitation wavelengths, emission colors, and Ln^{3+} ions compositions. This helps to predicate the chromaticity coordinates and guide preparation of complexes with desired photoluminescence. In addition, the unique characters, such as facile and controllable synthesis, versatile and reproducible Ln^{3+} isomorphous replacement, linearly tunable photoluminescence, infinite and predictable encoding combinations, and stable and easily detectable light output, offer promising potentials in barcoded materials applications by utilizing these kinds of multicolored photoluminescent mixed-Ln-MOFs.

EXPERIMENTAL SECTION

Materials and Methods. All reagents and solvents were purchased from J&K and Alfa Aesar and used without further purification. Physical methods for characterization, photophysical study, and crystallography are detailed in Supporting Information. See also CCDC 929635−929640, 929642.

Synthesis of Ligand. 1′,1″-(2,4,6-Trimethylbenzene-1,3,5-triyl)-tris(methylene)tris(pyridine-4(1*H*)-one) (TTP) was prepared as follows: under Ar atmosphere, 1,3,5-tri(bromomethyl)-trimethylbenzene (1.2 g, 3 mmol) was added to a suspension of 4-hydroxypyridine (0.95 g, 10 mmol) and K_2CO_3 (1.6 g, 12 mmol) in ethanol (30 mL). The reaction mixture was then refluxed at 80 °C for 24 h. On completion of the reaction, as indicated by thin-layer chromatography, the mixture was separated by filtration. The filtrate was evaporated at 40 °C under vacuum to give the crude product, which was washed with acetone three times and dried under vacuum overnight to give a pale yellow solid. Yield: 76%. ^{1}H NMR (300 MHz in D_2O): δ 2.13 (s, 9H, H_a), 5.31 (s, 6H, H_b), 6.39 (d, 6H, H_d), 7.54 (d, 6H, H_c). The molecular structure of TTP was identified by single-crystal diffraction measurement.

Synthesis of Complexes. To prepare monometallic complex $[\mathbf{Eu(TTP)_2H_2O}]\mathbf{Cl_3}\cdot C_3H_6O\cdot 9H_2O$ (**Eu-1**), a solution of TTP (14 mg, 0.03 mmol) in water (2 mL) was added to a stirred solution of $EuCl_3\cdot 6H_2O$ (7.3 mg, 0.02 mmol) in acetone (3 mL) at room temperature. After filtration, slow diffusion of acetone into the filtrate over 5 d afforded colorless crystals. Yield: 60%. Anal. Calcd for $C_{57}H_{78}Cl_3EuN_6O_{16}$: C, 50.28; H, 5.77; N, 6.17. Found: C, 49.93; H, 5.66; N, 6.33%.

$[\mathbf{Tb(TTP)_2H_2O}]\mathbf{Cl_3}\cdot C_3H_6O\cdot 11H_2O$ (**Tb-2**) was obtained by a similar procedure as for **1** except for using $TbCl_3\cdot 6H_2O$ instead of $EuCl_3\cdot 6H_2O$. Yield: 66%. Anal. Calcd for $C_{57}H_{84}Cl_3TbN_6O_{19}$: C, 48.12; H, 5.95; N, 5.91. Found: C, 48.02; H, 5.53; N, 6.00%. $[\mathbf{Gd(TTP)_2H_2O}]\mathbf{Cl_3}\cdot C_3H_6O\cdot 8H_2O$ (**Gd-3**) was obtained by a similar procedure as for **1** except for using $GdCl_3\cdot 6H_2O$ instead of $EuCl_3\cdot 6H_2O$. Yield: 60%. Anal. Calcd for $C_{57}H_{78}Cl_3GdN_6O_{16}$: C, 50.09; H, 5.75; N, 6.15. Found: C, 49.82; H, 5.54; N, 6.08%. The complexes **4**−**14** were obtanied by a similar procedure as for **1**, just changing the reactant stoichiometry of different Ln^{3+} ions as detailed in Supporting Information.

ASSOCIATED CONTENT

Supporting Information

Syntheses, characterization, photophysical details, correlation matrices, applications, and crystallographic data (CIF). This material is available free of charge via the Internet at http://pubs.acs.org.

AUTHOR INFORMATION

Corresponding Author

*E-mail: cesscy@mail.sysu.edu.cn.

Notes

The authors declare no competing financial interest.

ACKNOWLEDGMENTS

This work was supported by the 973 Program (2012CB821701), the NSFC Projects (91222201, 21173272, 21450110063), the NSF of Guangdong Province (S2013030013474), the RFDP of Higher Education of China (20120171130006), and the Fundamental Research Funds for the Central Universities. We thank J.-L. Schmitt and J.-M. Lehn of Université de Strasbourg for spectral measurement and helpful discussion.

REFERENCES

(1) (a) Muller, C. D.; Falcou, A.; Reckefuss, N.; Rojahn, M.; Wiederhirn, V.; Rudati, P.; Frohne, H.; Nuyken, O.; Becker, H.; Meerholz, K. *Nature* **2003**, *421*, 829−833. (b) Sava, D. F.; Rohwer, L. E. S.; Rodriguez, M. A.; Nenoff, T. M. *J. Am. Chem. Soc.* **2012**, *134*, 3983−3986. (c) Kokuoz, B.; DiMaio, J. R.; Kucera, C. J.; Evanoff, D. D.; Ballato, J. *J. Am. Chem. Soc.* **2008**, *130*, 12222−12223. (d) Eliseevaa, S. V.; Bünzli, J.-C. G. *Chem. Soc. Rev.* **2010**, *39*, 189−227. (e) Liu, D. M.; Lu, K. D.; Poon, C.; Lin, W. B. *Inorg. Chem.* **2014**, *53*, 1916−1924. (f) Meyer, L. V.; Schönfeld, F.; Müller-Buschbaum, K. *Chem. Commun.* **2014**, *50*, 8093−8108.

(2) White, K. A.; Chengelis, D. A.; Gogick, K. A.; Stehman, J.; Rosi, N. L.; Petoud, S. *J. Am. Chem. Soc.* **2009**, *131*, 18069−18071.

(3) (a) Schubert, E. F.; Kim, J. K. *Science* **2005**, *308*, 1274−1278. (b) Andrade, B. W. D.; Forrest, S. R. *Adv. Mater.* **2004**, *16*, 1585−1595. (c) Carlos, L. D.; Sa Ferreira, R. A.; Rainho, J. P.; De Zea Bermudez, V. *Adv. Funct. Mater.* **2002**, *12*, 819−823.

(4) (a) He, G. J.; Guo, D.; He, C.; Zhang, X. L.; Zhao, X. W.; Duan, C. Y. *Angew. Chem., Int. Ed.* **2009**, *48*, 6132−6135. (b) Wang, M.-S.; Guo, S.-P.; Li, Y.; Cai, L.-Z.; Zou, J.-P.; Xu, G.; Zhou, W.-W.; Zheng, F.-K.; Guo, G.-C. *J. Am. Chem. Soc.* **2009**, *131*, 13572−13573. (c) Liu, Y.; Pan, M.; Yang, Q.-Y.; Fu, L.; Li, K.; Wei, S.-C.; Su, C.-Y. *Chem. Mater.* **2012**, *24*, 1954−1960. (d) Yang, Q. Y.; Lehn, J. M. *Angew. Chem., Int. Ed.* **2014**, *53*, 4572−4577. (e) Evans, R. C.; Carlos, L. D.; Douglas, P.; Rocha, J. *J. Mater. Chem.* **2008**, *18*, 1100−1107. (f) Ki, W.; Li, J. *J. Am. Chem. Soc.* **2008**, *130*, 8114−8115. (g) Liao, Y.-C.; Lin, C.-H.; Wang, S.-L. *J. Am. Chem. Soc.* **2005**, *127*, 9986−9987.

(5) (a) Carlos, L. D.; Ferreira, R. A. S.; De Zea Bermudez, V.; Julián-López, B.; Escribano, P. *Chem. Soc. Rev.* **2011**, *40*, 536−549. (b) Bünzli, J.-C. G.; Piguet, C. *Chem. Soc. Rev.* **2005**, *34*, 1048−1077. (c) Bünzli, J.-C. G. *Chem. Rev.* **2010**, *110*, 2729−2755. (d) Petoud, S.; Cohen, S. M.; Bunzli, J.-C. G.; Raymond, K. N. *J. Am. Chem. Soc.* **2003**, *125*, 13324−13325. (e) Moore, E. G.; Samuel, A. P. S.; Raymond, K. N. *Acc. Chem. Res.* **2009**, *42*, 542−552. (f) Zhang, J.; Badger, P. D.; Geib, S. J.; Petoud, S. *Angew. Chem., Int. Ed.* **2005**, *44*, 2508−2512. (g) Zheng, X. L.; Liu, Y.; Pan, M.; Lv, X. Q.; Zhang, J. Y.; Zhao, C. Y.;

DOI: 10.1021/acs.inorgchem.5b00271
Inorg. Chem. 2015, 54, 5707−5716

Tong, Y. X.; Su, C. Y. *Angew. Chem., Int. Ed.* **2007**, *46*, 7399−7403. (h) Wei, Y. Q.; Li, Q. H.; Sa, R. J.; Wu, K. *Chem. Commun.* **2014**, *50*, 1820−1823. (i) Zhu, M.; Hao, Z.-M.; Song, X.-Z.; Meng, X.; Zhao, S.-N.; Song, S. Y.; Zhang, H.-J. *Chem. Commun.* **2014**, *50*, 1912−1914. (j) Zhang, S.-R.; Du, D.-Y.; Tan, K.; Qin, J.-S.; Dong, H.-Q.; Li, S.-L.; He, W.-W.; Lan, Y.-Q.; Shen, P.; Su, Z.-M. *Chem.—Eur. J.* **2013**, *19*, 11279−11286. (k) Zhang, Y.-H.; Li, X.; Song, S. *Chem. Commun.* **2013**, *49*, 10397−10399. (l) Dang, S.; Zhang, J.-H.; Sun, Z.-M. *J. Mater. Chem.* **2012**, *22*, 8868−8873. (m) Matthes, P. R.; Höller, C. J.; Mai, M.; Heck, J.; Sedlmaier, S. J.; Schmiechen, S.; Feldmann, C.; Schnickc, W.; Müller-Buschbaum, K. *J. Mater. Chem.* **2012**, *22*, 10179−10187.

(6) (a) Cui, Y.-J.; Yue, Y.-F.; Qian, G.-D.; Chen, B.-L. *Chem. Rev.* **2012**, *112*, 1126−1162. (b) Binnemans, K. *Chem. Rev.* **2009**, *109*, 4283−4374. (c) Allendorf, M. D.; Bauer, C. A.; Bhakta, R. K.; Houk, R. J. T. *Chem. Soc. Rev.* **2009**, *38*, 1330−1352. (d) Heine, J.; Müller-Buschbaum, K. *Chem. Soc. Rev.* **2013**, *42*, 9232−9242. (e) Cui, Y. J.; Chen, B. L.; Qian, G. D. *Coord. Chem. Rev.* **2014**, *273*−*274*, 76−86.

(7) (a) An, J.; Shade, C. M.; Chengelis-Czegan, D. A.; Petoud, S.; Rosi, N. L. *J. Am. Chem. Soc.* **2011**, *133*, 1220−1223. (b) Falcaro, P.; Furukawa, S. *Angew. Chem., Int. Ed.* **2012**, *51*, 8431−8433. (c) Jin, S. Y.; Son, H.-J.; Farha, O. K.; Wiederrecht, G. P.; Hupp, J. T. *J. Am. Chem. Soc.* **2013**, *135*, 955−958.

(8) (a) Zhang, X. J.; Ballem, M. A.; Hu, Z.-J.; Bergman, P.; Uvdal, K. *Angew. Chem., Int. Ed.* **2011**, *50*, 5729−5733. (b) Zhang, H. B.; Shan, X. C.; Zhou, L. J.; Lin, P.; Li, R. F.; Ma, E.; Guo, X. G.; Du, S. W. *J. Mater. Chem. C* **2013**, *1*, 888−891. (c) Ma, M.-L.; Ji, C.; Zang, S.-Q. *Dalton Trans.* **2013**, *42*, 10579−10586. (d) Le Natur, F.; Calvez, G.; Daiguebonne, C.; Guillou, O.; Bernot, K.; Ledoux, J.; Le Pollès, L.; Roiland, C. *Inorg. Chem.* **2013**, *52*, 6720−6730. (e) Tang, Q.; Liu, S. X.; Liu, Y. W.; He, D. F.; Miao, J.; Wang, X. Q.; Ji, Y. J.; Zheng, Z. P. *Inorg. Chem.* **2014**, *53*, 289−293. (f) Freslon, S.; Luo, Y.; Calvez, G.; Daiguebonne, C.; Guillou, O.; Bernot, K.; Michel, V.; Fan, X. *Inorg. Chem.* **2014**, *53*, 1217−1228. (g) Zhou, Y.; Yan, B. *Inorg. Chem.* **2014**, *53*, 3456−3463.

(9) (a) Zhao, D.; Seo, S.-J.; Bae, B.-S. *Adv. Mater.* **2007**, *19*, 3473−3479. (b) Wada, Y. J.; Sato, M.; Tsukahara, Y. *Angew. Chem., Int. Ed.* **2006**, *45*, 1925−1928. (c) Liu, Z.-F.; Wu, M.-F.; Wang, S.-H.; Zheng, F.-K.; Wang, G.-E.; Chen, J.; Xiao, Y.; Wu, A.-Q.; Guo, G.-C. *J. Mater. Chem. C* **2013**, *1*, 4634−4639. (d) Kerbellec, N.; Kustaryono, D.; Haquin, V.; Etienne, M.; Daiguebonne, C.; Guillou, O. *Inorg. Chem.* **2009**, *48*, 2837−2843. (e) Rao, X. T.; Huang, Q.; Yang, X. L.; Cui, Y. J.; Yang, Y.; Wu, C. D.; Chen, B. L.; Qian, G. D. *J. Mater. Chem.* **2012**, *22*, 3210−3214.

(10) (a) Rao, X. T.; Song, T.; Gao, J. K.; Cui, Y. J.; Yang, Y.; Wu, C. D.; Chen, B. L.; Qian, G. D. *J. Am. Chem. Soc.* **2013**, *135*, 15559−15564. (b) Cui, Y. J.; Xu, H.; Yue, Y. F.; Guo, Z. Y.; Yu, J. C.; Chen, Z. X.; Gao, J. K.; Yang, Y.; Qian, G. D.; Chen, B. L. *J. Am. Chem. Soc.* **2012**, *134*, 3979−3982.

(11) (a) De Lill, D. T.; De Bettencourt-Dias, A.; Cahill, C. L. *Inorg. Chem.* **2007**, *46*, 3960−3965. (b) Biju, S.; Raj, D. B. A.; Reddy, M. L. P.; Jayasankar, C. K.; Cowley, A. H.; Findlater, M. *J. Mater. Chem.* **2009**, *19*, 1425−1432. (c) Tremblay, M. S.; Halim, M.; Sames, D. *J. Am. Chem. Soc.* **2007**, *129*, 7570−7577. (d) Haquin, V.; Etienne, M.; Daiguebonne, C.; Freslon, S.; Calvez, G.; Bernot, K.; Le Pollès, L.; Ashbrook, S. E.; Mitchell, M. R.; Bünzli, J.-C.; Eliseeva, S. V.; Guillou, O. *Eur. J. Inorg. Chem.* **2013**, 3464−3476. (e) Zhang, H. B.; Shan, X. C.; Ma, Z. J.; Zhou, L. J.; Zhang, M. J.; Lin, P.; Hu, S. M.; Ma, E.; Li, R. F.; Du, S. W. *J. Mater. Chem. C* **2014**, *2*, 1367−1371.

(12) Yang, Q.-Y.; Li, K.; Luo, J.; Pan, M.; Su, C.-Y. *Chem. Commun.* **2011**, 4234−4236.

(13) (a) Han, X.; Wu, L. Z.; Si, G.; Pan, J.; Yang, Q. Z.; Zhang, L. P.; Tung, C. H. *Chem.—Eur. J.* **2007**, *13*, 1231−1239. (b) Yang, Q.-Y.; Wu, K.; Jiang, J.-J.; Hsu, C.-W.; Pan, M.; Lehn, J.-M.; Su, C.-Y. *Chem. Commun.* **2014**, *50*, 7702−7704.

(14) (a) Fukushima, T.; Horike, S.; Inubushi, Y.; Nakagawa, K.; Kubota, Y.; Takata, M.; Kitagawa, S. *Angew. Chem., Int. Ed.* **2010**, *49*, 4820−4824. (b) Sumida, K.; Stück, D.; Mino, L.; Chai, J.-D.; Bloch, E. D.; Zavorotynska, O.; Murray, L. J.; Dincă, M.; Chavan, S.; Bordiga, S.; Head-Gordon, M.; Long, J. R. *J. Am. Chem. Soc.* **2013**, *135*, 1083−1091.

(15) Aebischer, A.; Gumy, F.; Bünzli, J.-C. G. *Phys. Chem. Chem. Phys.* **2009**, *11*, 1346−1353.

DOI: 10.1021/acs.inorgchem.5b00271
Inorg. Chem. 2015, 54, 5707−5716